

Hierarchical Core-Shell N-Doped Carbon@FeP₄-CoP Arrays as Robust Bifunctional Electrocatalysts for Overall Water Splitting at High Current Density

Puxuan Yan, Yan Hu, Elvis Shoko, Tayirjan Taylor Isimjan,* Jianniao Tian, and Xiulin Yang*

Exploring non-precious metal-based electrocatalysts at high current density and stability is an urgent issue for sustainable H₂ production. Here, hierarchical core-shell N-doped carbon encapsulated array-like FeP₄ and CoP active components have been fabricated in situ on the surface of nickel foam (NC@FeP₄-CoP/NF) by etching sheet-like ZIF-67 arrays, Prussian analog formation, and phosphating in turns. The crystallinity, hierarchical heterostructure, and chemical state have been carefully discussed. Electrochemical studies demonstrate that the catalyst displays excellent electrocatalytic activity and durability in electrochemical oxygen evolution reaction ($\eta_{20} = 218$ mV) and hydrogen evolution reaction ($\eta_{10} = 116$ mV), better than most previously reported bifunctional catalysts. Moreover, the bifunctional catalyst only needs 1.72 and 1.80 V cell voltages at 500 and 1000 mA cm⁻² respectively, together with a good catalytic stability at 500 mA cm⁻² for 48 h, implying potential commercialization prospects. This excellent electrocatalytic performance is mainly attributed to the distinctive hierarchical structure as well as core-shell NC encapsulated FeP₄-CoP active sites, which can enhance the charge transport rate, inhibit the exfoliation of the active materials, provide a larger active surface area, and facilitate electrolyte diffusion and gas release.

1. Introduction

To mitigate the negative impacts of energy generation on climate and health, hydrogen is considered the most promising candidate to replace conventional fossil fuels.^[1] Offering a promising carbon-neutral path for hydrogen production, water splitting becomes one of the very promising strategies. The oxygen evolution reaction (OER) involves a sluggish four electron transfer procedure, it requires higher overpotential to overcome the energy barriers and enhance overall water splitting compared to the two-electron transfer process of the hydrogen evolution reaction (HER).^[2] Precious metal composites (Pt/C and RuO₂) have respectively exhibited the outstanding electrocatalytic activities for water splitting.^[3] But their scarcity and high cost limit their practical industrial application.^[4] Moreover, most of the HER and OER catalysts reported are limited by low current density.^[5] There is an urgent need to research earth-rich highly efficient cata-

lyst materials at large current density and durable performance for overall water splitting.


Metal-organic frameworks (MOF) are self-assembled crystalline material by metal salts and organic ligands,^[6] constituting ideal precursors for porous carbon-supported OER catalysts.^[7] These supported catalysts have high active surface area and porous channels, which can shorten electrolyte transport path during electrochemical reactions and display good stability,^[8] including Co@Co₃O₄/hollow N-doped carbon polyhedral,^[9] Co₃O₄/N-doped carbon,^[10] and CoO/CuO@N codoped carbon nanosheet.^[11] However, MOF-derived hybrids with suitable graphitic structures are normally obtained at relatively high temperatures (>800 °C),^[7] which favors the self-aggregation of bulk MOF phases, resulting in both the loss of active sites,^[12] and intensive energy consumption in the catalyst manufacturing process. Furthermore, in contrast to test electrodes prepared by bonding catalysts on a glassy carbon electrode,^[13] in situ catalyst growth on porous conductive carriers,^[14] such as nickel foam, carbon cloth, and carbon paper can yield more exposed active sites and/or enhance electrolyte and gas diffusion.^[6]

P. Yan, Y. Hu, Prof. J. Tian, Prof. X. Yang
Guangxi Key Laboratory of Low Carbon Energy Materials
School of Chemistry and Pharmaceutical Sciences
Guangxi Normal University
Guilin 541004, China
E-mail: xlyang@gxnu.edu.cn

P. Yan
Guangxi Key Laboratory of Information Materials
Guilin University of Electronic Technology
Guilin 541004, China

Dr. E. Shoko
Department of Chemistry
University of Liverpool
Liverpool L69 3BX, UK

Dr. T. T. Isimjan
Saudi Arabia Basic Industries Corporation (SABIC) at King Abdullah
University of Science and Technology (KAUST)
Thuwal 23955-6900, Saudi Arabia
E-mail: isimjant@sabic.com

 The ORCID identification number(s) for the author(s) of this article can be found under <https://doi.org/10.1002/admi.202100065>.

DOI: 10.1002/admi.202100065

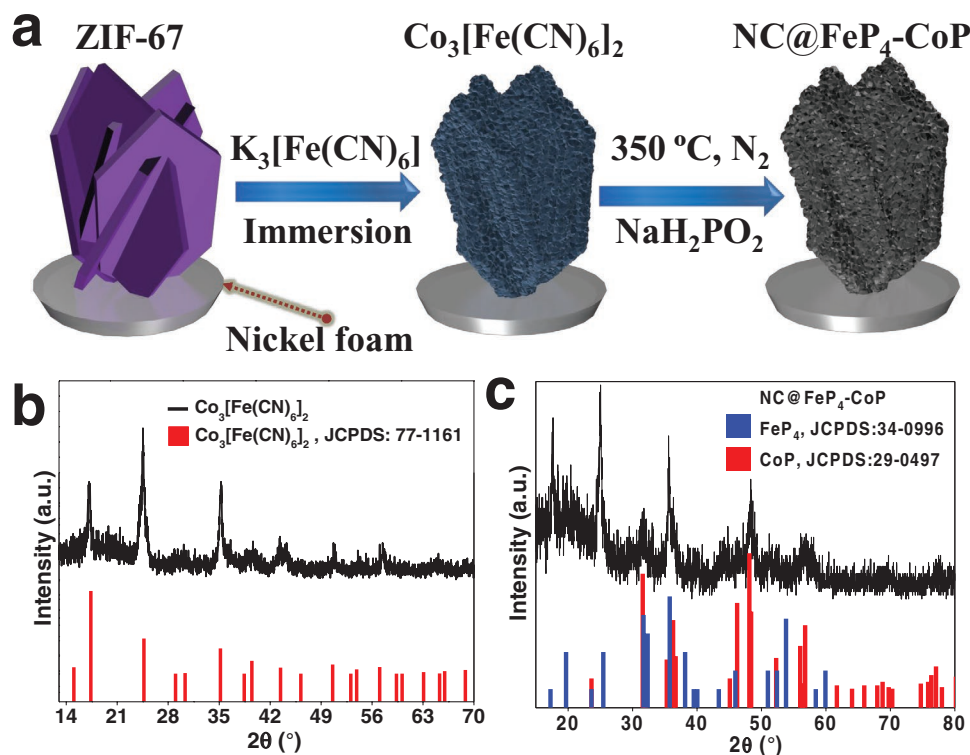


Figure 1. a) Schematic synthesis process of NC@FeP₄-CoP/NF. X-ray diffraction (XRD) patterns of b) Co₃[Fe(CN)₆]₂/NF and c) NC@FeP₄-CoP/NF.

These desirable functional properties of porous conductive carriers could be harnessed to develop highly efficient transition metal phosphide catalysts for electrochemical applications. In contrast to transition metal oxides, transition metal phosphides exhibit metalloid characteristics of good electrical conductivity and chemical stability,^[1b,15] along with an optimized hydrogen binding energy,^[16] yielding high electrocatalytic activities toward HER. Transition metal phosphides, such as FeP/Ni₂P,^[15] CoP,^[17] Ni-CoP@C,^[18] and NiCoP,^[19] show simultaneous activity for both HER and OER, a feature that is particularly true for the cobalt phosphides.^[1b] Nonetheless, metal phosphides still exhibit a relatively high overpotential for the OER, an important limitation for these catalyst systems that must be overcome in order to unlock their potential for industrial application. Previous research has shown that careful nanostructuring of these catalyst systems to expose lots of active sites is a particularly effective strategy to partially alleviate this limitation by reducing the charge transfer resistance.^[1b] Therefore, developing gentle preparation routes to fabricate transition metal phosphides on porous conductive carriers that allow controllable nanostructuring is an important research direction for water splitting technologies.

Herein, we have developed an efficient strategy for constructing hierarchical core-shell N-doped carbon encapsulated CoP and FeP₄ arrays on nickel foam (NC@FeP₄-CoP/NF). The as-prepared catalyst was fabricated by in situ growth ZIF-67 sheet array on NF skeleton, etching formation of Prussian analog, as well as an additional phosphating process. The resulted composite shows a unique array-like structure composed of core-shell components. According to our

electrochemical results, the NC@FeP₄-CoP/NF catalyst has the smallest overpotential (218 mV) at 20 mA cm⁻² as well as the lowest Tafel slope (50.9 mV dec⁻¹) among the other catalyst including NC@CoP/NF (258 mV), RuO₂/NF (279 mV), and most previously reported similar catalysts. The outstanding catalytic performance is attributed to the unique synergy between Fe and Co species resulted in array-like morphology and a better charge transfer. In addition, the optimized NC@FeP₄-CoP/NF also shows good stability under the simulated industrial high current density.

2. Results and Discussion

The fabrication procedure of NC@FeP₄-CoP/NF is presented in **Figure 1a**. First, the blue purple ZIF-67 sheet is uniformly constructed on NF skeleton by immersion of the NF in the mixed solution of Co(NO₃)₂ and 2-methylimidazole. According to Figure S2, Supporting Information, the ZIF-67 is unstable in water but stable in pure ethanol during the 12 h due to hydrogen ions.^[20] When potassium ferricyanide aqueous solution was mixed with ZIF-67 ethanol suspension, the gray green of the mixture gradually changes into brown (Figure S3, Supporting Information), explaining that the as-prepared ZIF-67 was slowly dissociated into cobalt ions in the water.^[21] Meanwhile, the dissociated cobalt ions and ferricyanide ions in the mixed solution react in situ to synthesize Co₃[Fe(CN)₆]₂. After further immersion for 12 h at room temperature, the ZIF-67 is completely transformed into Co₃[Fe(CN)₆]₂ on the NF, where the Co and Fe atoms are distributed at the atomic level in the bimetallic

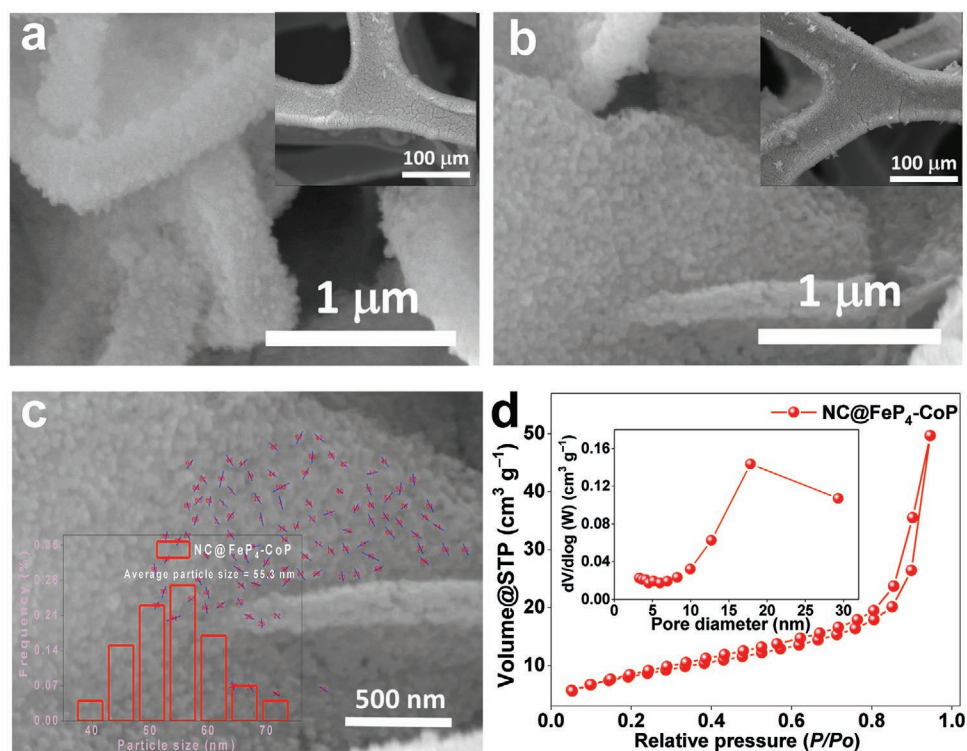


Figure 2. a) Scanning electron microscopy (SEM) images of $\text{Co}_3[\text{Fe}(\text{CN})_6]_2/\text{NF}$. SEM and high-magnification SEM images of b) $\text{NC}@FeP_4\text{-CoP}/\text{NF}$, and c) particle size distribution of $\text{NC}@FeP_4\text{-CoP}$. d) Nitrogen adsorption–desorption isotherms of $\text{NC}@FeP_4\text{-CoP}$.

organic complex of $\text{Co}_3[\text{Fe}(\text{CN})_6]_2$ which allows a uniform phosphatization.^[22] Studies have shown that Prussian analog is a stable complex, and the structure will not collapse during high-temperature pyrolysis.^[23] During the subsequent phosphating treatment, $\text{Co}_3[\text{Fe}(\text{CN})_6]_2$ can be decomposed and react with PH_3 to form FeP_4 and CoP ,^[22] while CN^- coordination ions are pyrolyzed into N-doped carbon materials (Table S1, Supporting Information) and interwoven over the surface of active species. The loading of $\text{NC}@FeP_4\text{-CoP}$ on NF is $\approx 7.4 \text{ mg cm}^{-2}$. As a comparison, $\text{NC}@CoP$, RuO_2 and Pt/C loading on NF are respectively 7.9, 2.0, and 1.0 mg cm^{-2} .

The transformation of the crystal structure of species was analyzed by XRD. It can be observed from Figure S4, Supporting Information that the pattern of ZIF-67 on NF skeleton exactly matches that of ZIF-67 previously published in the literatures.^[24] After soaking in ferricyanide ion solution, the ZIF-67 is in situ transformed into $\text{Co}_3[\text{Fe}(\text{CN})_6]_2$ (JCPDS: 23–0189) (Figure 1b). After sufficient phosphating treatment, ZIF-67 can be converted into $\text{NC}@CoP$ (JCPDS: 29–0497) (Figure S5, Supporting Information), while $\text{Co}_3[\text{Fe}(\text{CN})_6]_2$ can be completely phosphated into orthorhombic CoP (JCPDS: 29–0497) along with orthorhombic FeP_4 (JCPDS: 34–0996) in $\text{NC}@FeP_4\text{-CoP}$ composite (Figure 1c), which was further confirmed by transmission electron microscopy (TEM). The high noise-to-signal is mostly due to the low crystallinity of the phosphide.^[25]

We used scanning electron microscopy (SEM) to observe the material microstructure. It can be seen from Figure S6, Supporting Information that ZIF-67 completely covers the surface of NF, and the high-resolution SEM shows a crisscrossed sheet structure with a thickness of $\approx 154 \text{ nm}$. After converting

ZIF-67/NF to $\text{Co}_3[\text{Fe}(\text{CN})_6]_2/\text{NF}$, the smooth sheet structure is transformed into an array structure composed of many particulate structures, (Figure 2a). After phosphating, there is almost no change in the catalyst morphology (Figure 2b). The high magnification SEM image of $\text{NC}@FeP_4\text{-CoP}/\text{NF}$ reveals that the average particle size is $\approx 55.3 \text{ nm}$ according to the size distribution of 100 particles (Figure 2c). On the contrary, the structure of the $\text{NC}@CoP/\text{NF}$ after phosphating of ZIF-67/NF has collapsed significantly (Figure S7, Supporting Information). The four-probe test showed that the conductivity of $\text{NC}@FeP_4\text{-CoP}/\text{NF}$ was 1727 S cm^{-1} (Table S2, Supporting Information), indicating good conductivity.

The surface area and porosity of as-synthesized $\text{NC}@FeP_4\text{-CoP}$ and $\text{NC}@CoP$ were measured using the N_2 adsorption-desorption isotherm experiments. The obtained curve is consistent with a typical III-type isotherm with hysteresis loop. The specific surface area of hierarchical $\text{NC}@FeP_4\text{-CoP}$ is $29.4 \text{ m}^2 \text{ g}^{-1}$, which is much higher than that of $\text{NC}@CoP$ ($3.0 \text{ m}^2 \text{ g}^{-1}$) (Figure S8, Supporting Information). Its average pore size is 178 nm (Figure 2d). The role of ZIF-67 is a hard template where the Co and Fe atoms are closely compacted therefore easier to form a film on the surface through thermal annealing and easy to create controllable porous surface morphology. The high specific surface area and mesoporous properties help to accelerate the transport of electrolyte and gas emission,^[26] thereby improving electrocatalytic performance.

TEM of $\text{NC}@FeP_4\text{-CoP}$ after ultrasonic exfoliation indicates that the particulate FeP_4 and CoP are well-distributed in the framework of the NC composite (Figure 3a). The high-resolution TEM images show the FeP_4 and CoP particles around 10 nm in

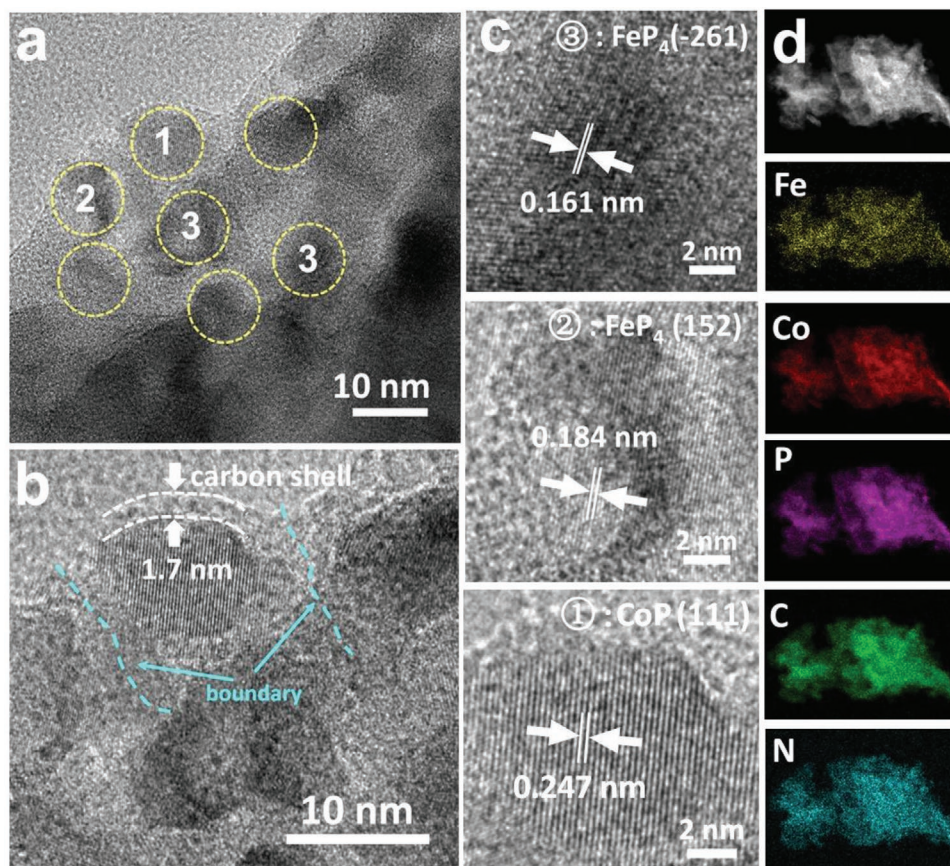


Figure 3. a) Transmission electron microscopy (TEM) and b) High-resolution TEM images of NC@FeP₄-CoP. c) HAADF-STEM images of NC@FeP₄-CoP and d) elemental mappings of Co, Fe, P, C, and N, respectively.

size which were encapsulated by a 1.7 nm NC shell (Figure 3b). The nano-level dispersion of two species generates a sufficient interface that promotes the charge transfer through the conductive NC shell consequently better efficiency as compared to CoP. This structure can provide higher electronic conductivity (Table S2, Supporting Information) and can effectively inhibit the peeling of the active material, thereby improving the long-term stability of the catalytic material.^[2a] As shown in Figure 3c, a clear set of 0.247 nm interplanar distances belong to the (111) crystal plane of monoclinic CoP,^[1b,27] and the other two types of interplanar distances (0.184 and 0.161 nm) respectively belong to the (152) and (-261) crystal planes of orthorhombic FeP₄.^[28] In addition, the elemental mappings about NC@FeP₄-CoP explain that Co, Fe, P, C, and N elements are evenly dispersed in the entire structure of NC@FeP₄-CoP (Figure 3d).

The chemical state of surface elements in NC@FeP₄-CoP was further checked by XPS. The survey spectrum reveals NC@FeP₄-CoP contains Fe, Co, P, C, and N elements (Figure S9a, Supporting Information). Based on carbon species obtained through Prussian blue analog phosphating,^[29] we deconvolute the high resolution C 1s range to C=C (284.0 eV), C-C (284.8 eV), and C-N/C-O (286.1 eV) (Figure S9b, Supporting Information).^[30] In the Co 2p_{3/2} range, the binding energies at 778.6, 780.9, and 783.7 eV are ascribed to the Co phosphating species, partially oxidized Co species, and the satellite peak, respectively (Figure 4a).^[17,31] In the Fe 2p_{3/2} range,

The spectrum is divided into four main peaks (Figure 4b), of which a small peak at 706.8 eV can be attributed to the Fe-P bond derived from FeP₄,^[32] and the binding energy at 708.3 eV corresponds to the Fe(III) species,^[33] and two peaks at 712.4 and 714.7 eV belong to satellite peaks. As shown in Figure 4c, there are three peaks mainly identified as P-O and metal-P chemical bonds, among which the peak of 133.8 eV represents the P-O bond generated due to phosphorus surface oxidation, and two peaks at 129.4 and 130.3 eV are consistent with P 2p_{3/2} and P 2p_{1/2} of metal-P bonds.^[1b] In Figure 4d, two strong peaks at 397.2 and 401.1 eV can be respectively assigned to pyridine nitrogen and graphite nitrogen in the N 1s range.^[33,34]

The OER performance of various catalysts was evaluated by using a three-electrode system in 1.0 M KOH. It can be seen from Figure 5a that as the overpotential increases, there is an oxidation peak that converts low valence of Co to high valence between 0 and 0.2 V, and then the OER current density increases rapidly, the corresponding overpotential at 10 mA cm⁻² difficult to identify, due to the peak valley appeared at the same position therefore the overpotentials at 20 mA cm⁻² is used instead for comparison. We can observe that the overpotentials of NC@FeP₄-CoP/NF only need 218 mV (20 mA cm⁻²) and 255 mV (100 mA cm⁻²), which is far better than other designed catalysts and most previously published catalysts (Table S3, Supporting Information). Notably, the NC@FeP₄-CoP/NF (218 mV@20 mA cm⁻²) catalyst performs much

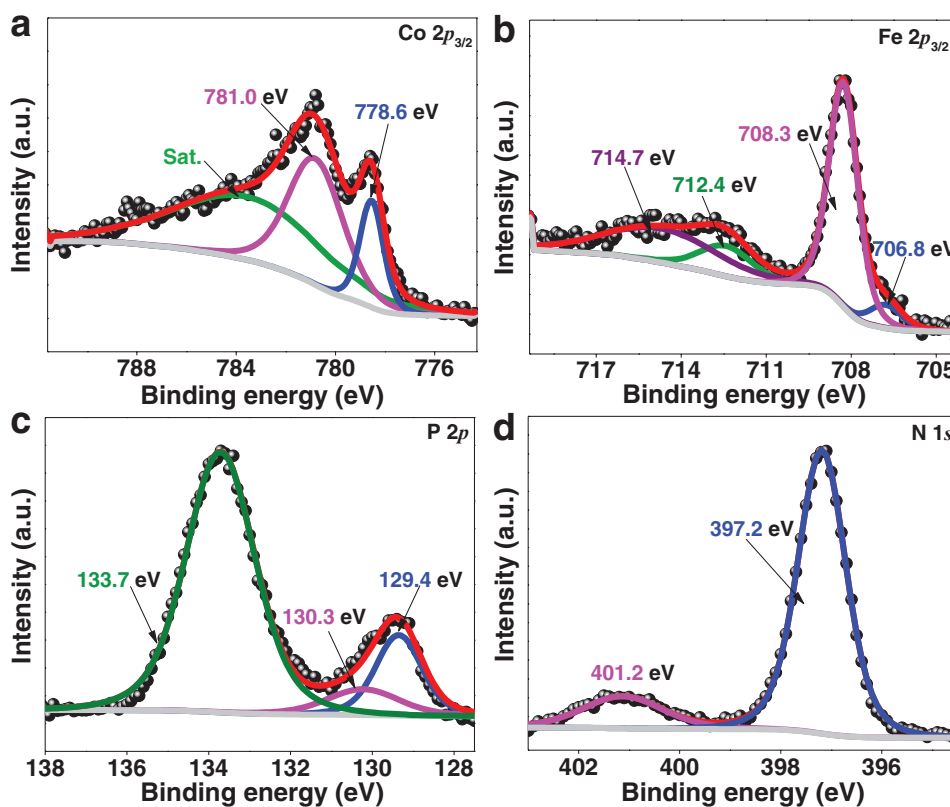


Figure 4. High-resolution XPS spectra of a) Co $2p_{3/2}$, b) Fe $2p_{3/2}$, c) P $2p$, and d) N $1s$ for NC@FeP₄-CoP/NF.

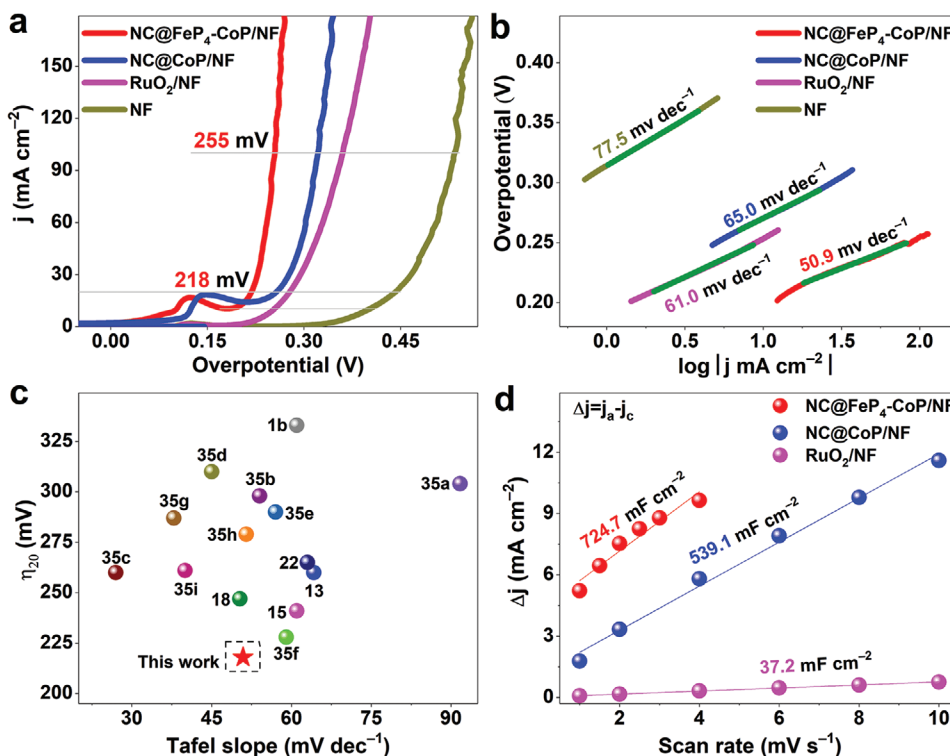


Figure 5. a) LSV polarization curves of NC@FeP₄-CoP/NF along with various control catalysts for OER. b) Tafel plots of various catalysts from (a). c) A summary diagram of Tafel slopes and overpotentials at 20 mA cm⁻² of different catalysts reported recently.^[1b,13,15,18,22,35] d) The summarized C_{dl} from CV curves with different scan rates in a non-Faradaic potential region.

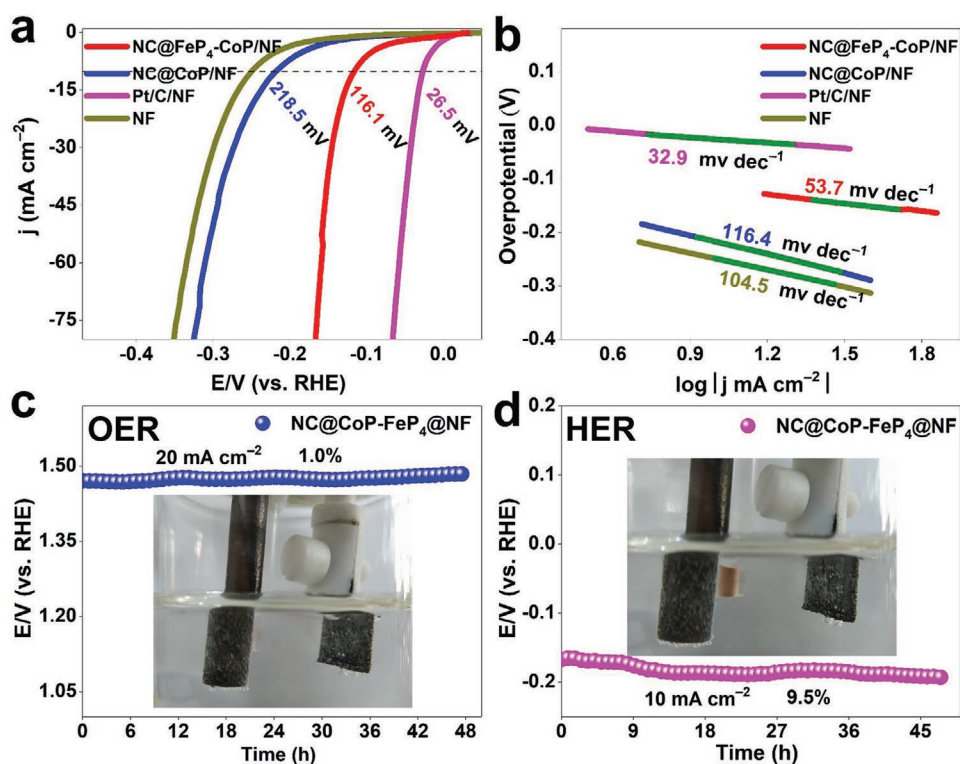


Figure 6. a) LSV polarization curves of NC@FeP₄-CoP/NF, NC@CoP/NF, Pt/C/NF, and NF for HER. b) Tafel plots of various catalysts from (a). Chronopotentiometry curves of NC@FeP₄-CoP/NF for c) OER and d) HER at the different current densities.

better than that of NC@FeCoO_x/NF (301 mV@20 mA cm⁻²) (Figure S10, Supporting Information), indicating the importance of forming metal phosphide. As shown in Figure 5b, the Tafel slope (50.9 mV dec⁻¹) of NC@FeP₄-CoP/NF is smaller than those of NC@CoP/NF (65.0 mV dec⁻¹) and RuO₂/NF (61.0 mV dec⁻¹), indicating a faster OER catalytic kinetics.^[34,36] In alkaline solution, the widely reported OER catalytic mechanism is carried out by four intermediates of *OH, *O, *OOH, and O₂ on the active site.^[37] The loading of RuO₂/NF on the surface of NF is ≈2 mg cm⁻². We compare NC@FeP₄-CoP/NF with similar catalysts published recently and show them in Figure 5c. It can be noted that the catalysts developed in this work have outstanding advantages in these two aspects, implying that it has a good prospect of industrial application. As we discuss shortly, the outstanding electrocatalytic capability is closely related to the faster charge transport speed and the larger electrochemically active surface area (ECSA). The Nyquist diagram was obtained by electrochemical impedance spectrum. As shown in Figure S11, Supporting Information, the smaller semicircle diameter, the faster the charge transport speed of the electrode.^[14] Compared with others, the NC@FeP₄-CoP/NF has a smaller semicircle diameter, indicating a faster charge transfer capability, which can be attributed to the catalyst with unique NC shell and array structure, effectively shortening the ion diffusion path.^[38] Many studies have found that the ECSA increases as the electrochemical double layer capacitance (C_{dl}) increase.^[15] The C_{dl} of NC@FeP₄-CoP/NF is 724.7 mF cm⁻², it is ≈1.3 and 19.6 times higher than NC@CoP/NF and RuO₂/NF catalysts (Figure 5d, Figure S12, Supporting Information).

This result is attributed to the catalyst hierarchical structure that can expose more active sites. Furthermore, the NC@FeP₄-CoP/NF catalyst shows a high turnover frequency (TOF). For example, NC@FeP₄-CoP/NF can obtain a 0.011 s⁻¹ TOF value at lower overpotential of 276 mV (Figure S13 and Table S4, Supporting Information), than the 350 mV overpotential of NC@CoP/NF, indicating that NC@FeP₄-CoP/NF has better intrinsic activity.^[39]

The NC@FeP₄-CoP/NF catalyst was further evaluated about HER properties via linear sweep voltammetry (LSV) curves. This catalyst shows a lower overpotential of 116 mV at 10 mA cm⁻² in 1.0 M KOH, it is superior to the control NC@CoP/NF (218 mV) and NF (249 mV) catalysts (Figure 6a). Figure 6b shows that the Tafel slope of NC@FeP₄-CoP/NF is 53.7 mV dec⁻¹, revealing that the HER process by NC@FeP₄-CoP/NF electrode proceeds through the Volmer-Heyrovsky mechanism,^[40] where H⁺ ion is adsorbed on the surface of NC@FeP₄-CoP to form the H* species, then one H* combines with a H⁺ and an electron to form H₂ molecule.^[41] The stability study of the three-electrode system has important guiding significance for evaluating the catalyst potential for industrial application. In 1.0 M KOH, Figure 6c is a long-term stability study of NC@FeP₄-CoP/NF catalyst at a constant of 20 mA cm⁻². The average relative deviation of OER catalytic stability has only declined by ≈1% after 48 h of continuous operation, showing outstanding stability. The XPS (Figure S14, Supporting Information) and SEM (Figure S15, Supporting Information) analyses were performed on the catalyst after long-term stability testing. The SEM result indicates a minor change in the morphology but

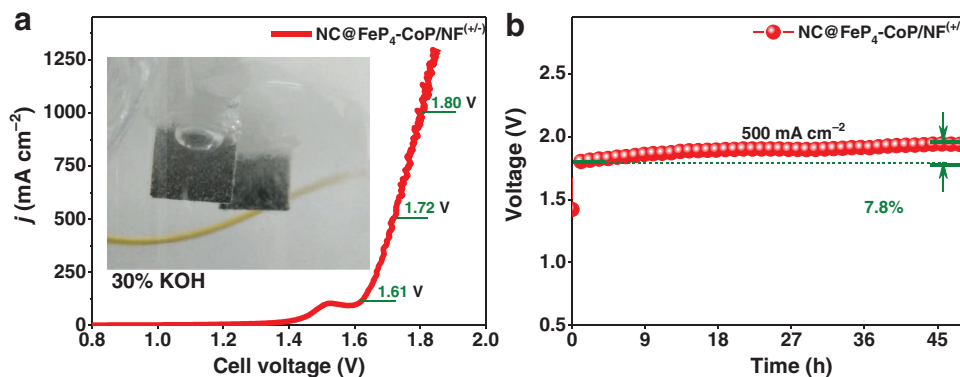


Figure 7. a) Overall water splitting study of NC@FeP₄-CoP/NF^(+/) as a bifunctional catalyst in 30 wt% KOH solution. b) Durability test of NC@FeP₄-CoP/NF^(+/) at 500 mA cm⁻² in a simulated industrialized two-electrode system.

on the other hand, the XPS shows completely different surface properties as compared to as-prepared samples, for example, the P was mostly oxidized and Fe and Co positions were shifted. However, new (oxy)hydroxide species appeared on the surface which is widely reported as the actual active sites of metal phosphide OER catalyst.^[42] Similar catalytic stability is also observed in the long-term stability study of the HER (Figure 6d). Due to the unique structure of the hybrid catalyst, it can be seen that the voltage of NC@FeP₄-CoP/NF catalyst has declined by ≈9.5% after running for 48 h at -10 mA cm⁻², that is, the carbon-encapsulated NC shell can effectively reduce the exfoliation of catalytically active particles and also regulate the adsorption energy of the product gas thereby facilitating its release.

To meet the needs of industrial applications, the overall water splitting activity of NC@FeP₄-CoP/NF^(+/) was studied in a typical two-electrode system. Initially, we explored a NC@FeP₄-CoP/NF bifunctional catalyst for overall water splitting in 1.0 M KOH, it is found that it only needs a total voltage of 1.68 V at 20 mA cm⁻², which is better than most previously published similar catalysts (Figure S16, Supporting Information). More importantly, since industrialized overall water splitting is mostly performed in 30 wt% KOH solution and is operated under high current density greater than 500 mA cm⁻²,^[43] we further studied the performance of bifunctional NC@FeP₄-CoP/NF^(+/) catalyst under simulated industrial demand. The required total voltages of NC@FeP₄-CoP/NF^(+/) catalyst are 1.61, 1.72, and 1.80 V at 100, 500, and 1000 mA cm⁻² in 30 wt% KOH (Figure 7a), respectively. This result is superior to RuO₂⁽⁺⁾/NiS_x-MoO₂⁽⁻⁾ and RuO₂⁽⁺⁾/Pt/C⁽⁻⁾ under similar reaction conditions as we previously reported.^[40] Moreover, when the two-electrode system of NC@FeP₄-CoP/NF^(+/) is operated for 48 h at 500 mA cm⁻², the stability study shows that the total voltage only increases by ≈7.8% (Figure 7b), showing good prospects for industrial application.

3. Conclusions

In conclusion, we have designed a controllable method of hierarchical core-shell N-doped carbon encapsulated FeP₄-CoP active nanoparticle arrays on nickel foam skeleton. XRD explored the crystal structure, SEM and TEM analyzed the

microstructure, BET confirmed the porosity, and XPS analyzed the surface chemical state of the hybrid material. Electrochemical OER indicates that the NC@FeP₄-CoP/NF catalyst only needs 218 and 250 mV overpotentials at 20 and 100 mA cm⁻², accompanied by a small Tafel slope, low charge transfer impedance, large C_{dl}, and outstanding stability, they are better than most previously published catalysts. Meanwhile, the electrochemical HER also shows good electrocatalytic activity and stability, showing excellent functional overall water splitting characteristics. Specifically, the NC@FeP₄-CoP/NF catalyst only requires cell voltages of 1.61, 1.72, and 1.80 V at 100, 500, and 1000 mA cm⁻² respectively, along with long-term large-current stability, demonstrating good prospects for commercial application. Based on overall water splitting, the proposed synthesis strategy may provide the possibility to develop facile and durable electrocatalysts in industrial applications.

4. Experimental Section

Synthesis of ZIF-67 and Co₃[Fe(CN)₆]₂/NF: The ZIF-67/NF composite was prepared according to our previously reported work.^[44] Then, 20 mg of K₃[Fe(CN)₆] was dissolved in 20 mL of deionized water in a beaker, and the ZIF-67/NF was immersed in 20 mL of ethanol in another beaker. After that, the K₃[Fe(CN)₆] solution was poured into the ethanol solution containing the ZIF-67/NF, and left for 12 h at room temperature. The resulted sample was then taken out, rinsed with abundant water, and dried in an oven at 38 °C for 12 h. The resulting dark blue sample was nominated as Co₃[Fe(CN)₆]₂/NF.

Synthesis of NC@FeP₄-CoP/NF and NC@CoP/NF: The phosphidation process was performed in a tube furnace, where the NaH₂PO₂ was located in the upstream side and the Co₃[Fe(CN)₆]₂/NF was located next to the NaH₂PO₂ at a downstream side. The temperature was raised to 350 °C at 5 °C min⁻¹, and kept for 3 h under an Ar gas flow. The resulting samples with black color were designated as NC@FeP₄-CoP/NF. As a control, black NC@CoP/NF was also prepared by the similar phosphating method as described above. In addition, RuO₂/NF and Pt/C/NF were also prepared according to the previously reported method,^[44] in which the loading of RuO₂ and Pt/C were set to 2 and 1 mg cm⁻², respectively.

Electrochemical Measurements: The electrocatalytic activity for OER was measured by a standard three-electrode system of electrochemical workstation (Biologic VMP3) with 1.0 M KOH (pH = 13.5) as the electrolyte. The prepared samples were used as the working electrode. The reference electrode and the counter electrode were a saturated calomel electrode (SCE) and a carbon rod, respectively. Before tests, the

catalysts were cycled several times via cyclic voltammetry (CV) between 0 and 0.8 V. LSV was carried out at a scan rate of 2 mV s⁻¹.

The potential of E_{RHE} was calibrated by the equation of $E_{\text{RHE}} = E_{\text{SCE}} + 0.241 + 0.059\text{pH} = E_{\text{SCE}} + 1.037$, which was consistent with the RHE voltage calibration result of 1.037 V (Figure S1, Supporting Information). All the LSV polarization curves were corrected by the equation of $E_{\text{cor}} = E_{\text{RHE}} - iR_s$, where E_{cor} was the corrected potential (V), i was the test current (A), and R_s was the solution resistance obtained from electrochemical impedance spectroscopy (EIS, Ω). The EIS measurements were performed at 1.54 V (versus RHE) with frequencies from 200 kHz to 0.1 Hz. The stability of the samples was investigated by chronopotentiometry at varying current densities of 10, 20, and 500 mA cm⁻², respectively.

The double layer capacitance (C_{dl}) of all catalysts were studied in a potential window with non-faradaic current in 1.0 M KOH. The scan rates were in the range of 1 to 10 mV s⁻¹, and the C_{dl} was calculated by the equation of $C_{\text{dl}} = (j_a - j_c)/(2 \times v)$, where j_a and j_c were the respective current density of anode and cathode, and v is the scan rate.

Overall Water Splitting: The overall water splitting of the two electrodes was first carried out in 1.0 M KOH solution. In this process, the designed NC@FeP₄-CoP/NF^(+/·) catalyst acted as a bifunctional catalyst for both cathode and anode electrodes. Then, the evaluation of the bifunctional catalyst was continued in a 30 wt% KOH solution that simulated industrial application conditions. The electrocatalytic activity and stability of the bifunctional catalyst were particularly explored under high current density conditions.

Supporting Information

Supporting Information is available from the Wiley Online Library or from the author.

Acknowledgements

P.Y. and Y.H. contributed equally to this work. This work has been supported by the National Natural Science Foundation of China (no. 21965005), Natural Science Foundation of Guangxi Province (2018GXNSFAA294077, 2018GXNSFAA281220), Guangxi Key Laboratory of Information Materials (171033-Z), Project of High-Level Talents of Guangxi (F-KA18015, 2018ZD004), Innovation Project of Guangxi Graduate Education (XYCSZ2019056, YCBZ2019031), and Guangxi Technology Base and Talent Subject (GUIKE AD18126001).

Conflict of Interest

The authors declare no conflict of interest.

Data Availability Statement

The data that support the findings of this study are available from the corresponding author upon reasonable request.

Keywords

bifunctional catalysis, FeP₄-CoP, hierarchical structures, metal-organic frameworks, water splitting

Received: January 15, 2021

Revised: March 13, 2021

Published online:

- [1] a) W. Xiong, Q. Guo, Z. Guo, H. Li, R. Zhao, Q. Chen, Z. Liu, X. Wang, *J. Mater. Chem. A* **2018**, *6*, 4297; b) M. Song, Y. He, M. Zhang, X. Zheng, Y. Wang, J. Zhang, X. Han, C. Zhong, W. Hu, Y. Deng, *J. Power Sources* **2018**, *402*, 345; c) Q. Zhou, T.-T. Li, J. Qian, Y. Hu, F. Guo, Y.-Q. Zheng, *J. Mater. Chem. A* **2018**, *6*, 14431.
- [2] a) L.-M. Cao, D. Lu, D.-C. Zhong, T.-B. Lu, *Coord. Chem. Rev.* **2020**, *407*, 213156; b) T. Kou, S. Wang, J. L. Hauser, M. Chen, S. R. J. Oliver, Y. Ye, J. Guo, Y. Li, *ACS Energy Lett.* **2019**, *4*, 622.
- [3] a) Y. Liu, S. Jiang, S. Li, L. Zhou, Z. Li, J. Li, M. Shao, *Appl. Catal., B* **2019**, *247*, 107; b) C. Li, B. Zhang, Y. Li, S. Hao, X. Cao, G. Yang, J. Wu, Y. Huang, *Appl. Catal., B* **2019**, *244*, 56.
- [4] Z. Kou, L. Zhang, Y. Ma, X. Liu, W. Zang, J. Zhang, S. Huang, Y. Du, A. K. Cheetham, J. Wang, *Appl. Catal., B* **2019**, *243*, 678.
- [5] D. Senthil Raja, C.-L. Huang, Y.-A. Chen, Y. Choi, S.-Y. Lu, *Appl. Catal., B* **2020**, *279*, 119375.
- [6] Z. Hao, X. Jiaying, J. Yiwen, T. YinLin, L. Qingyi, G. Feng, *Chem. - Eur. J.* **2018**, *24*, 5562.
- [7] J. Du, G. Liu, F. Li, Y. Zhu, L. Sun, *Adv. Sci.* **2019**, *6*, 1900117.
- [8] H. Tan, J. Tang, J. Henzie, Y. Li, X. Xu, T. Chen, Z. Wang, J. Wang, Y. Ide, Y. Bando, Y. Yamauchi, *ACS Nano* **2018**, *12*, 5674.
- [9] D. Ding, K. Shen, X. Chen, H. Chen, J. Chen, T. Fan, R. Wu, Y. Li, *ACS Catal.* **2018**, *8*, 7879.
- [10] Y. Xiaobing, C. Juan, C. Yuqing, F. Pingjing, L. Huixian, L. Jintang, L. Xuetao, *Nano-Micro Lett.* **2017**, *10*, 15.
- [11] X. Kuang, Z. Wang, X. Sun, Y. Zhang, Q. Wei, *Chem. Commun.* **2018**, *54*, 264.
- [12] a) D. Zhang, W. Chen, Z. Li, Y. Chen, L. Zheng, Y. Gong, Q. Li, R. Shen, Y. Han, W.-C. Cheong, L. Gu, Y. Li, *Chem. Commun.* **2018**, *54*, 4274; b) J. Zhou, Y. Dou, A. Zhou, L. Shu, Y. Chen, J.-R. Li, *ACS Energy Lett.* **2018**, *3*, 1655.
- [13] H. Wang, Y. Li, R. Wang, B. He, Y. Gong, *Electrochim. Acta* **2018**, *284*, 504.
- [14] A. T. A. Ahmed, B. Hou, H. S. Chavan, Y. Jo, S. Cho, J. Kim, S. M. Pawar, S. Cha, A. I. Inamdar, H. Kim, H. Im, *Small* **2018**, *14*, 1800742.
- [15] Y. Feng, C. Xu, E. Hu, B. Xia, J. Ning, C. Zheng, Y. Zhong, Z. Zhang, Y. Hu, *J. Mater. Chem. A* **2018**, *6*, 14103.
- [16] a) L. Huiming, L. Siqi, S. Jingyao, P. Jiajing, L. Di, X. Yanrong, M. Junjie, Z. Wei, Z. Zhongbin, *Chem. - Eur. J.* **2018**, *24*, 1; b) J. Ma, Y. Wang, W. Pan, J. Zhang, *Chem. - Asian J.* **2020**, *15*, 00229.
- [17] Y. Dang, J. He, T. Wu, L. Yu, P. Kerns, L. Wen, J. Ouyang, S. L. Suib, *ACS Appl. Mater. Interfaces* **2019**, *11*, 29879.
- [18] X. Han, C. Yu, H. Huang, W. Guo, C. Zhao, H. Huang, S. Li, Z. Liu, X. Tan, Z. Gao, J. Yu, J. Qiu, *Nano Energy* **2019**, *62*, 136.
- [19] Z. Fang, L. Peng, Y. Qian, X. Zhang, Y. Xie, J. J. Cha, G. Yu, *J. Am. Chem. Soc.* **2018**, *140*, 5241.
- [20] Y. Zeng, G.-F. Chen, Z. Jiang, L.-X. Ding, S. Wang, H. Wang, *J. Mater. Chem. A* **2018**, *6*, 15942.
- [21] J.-F. Qin, J.-Y. Xie, N. Wang, B. Dong, T.-S. Chen, Z.-Y. Lin, Z.-Z. Liu, Y.-N. Zhou, M. Yang, Y.-M. Chai, *J. Colloid Interface Sci.* **2020**, *562*, 279.
- [22] C. Du, L. Yang, F. Yang, G. Cheng, W. Luo, *ACS Catal.* **2017**, *7*, 4131.
- [23] L.-M. Cao, Y.-W. Hu, S.-F. Tang, A. Iljin, J.-W. Wang, Z.-M. Zhang, T.-B. Lu, *Adv. Sci.* **2018**, *5*, 1800949.
- [24] a) X. Guo, T. Xing, Y. Lou, J. Chen, *J. Solid State Chem.* **2016**, *235*, 107; b) W. Sun, X. Zhai, L. Zhao, *Chem. Eng. J.* **2016**, *289*, 59.
- [25] C. Xuan, J. Wang, W. Xia, Z. Peng, Z. Wu, W. Lei, K. Xia, H. L. Xin, D. Wang, *ACS Appl. Mater. Interfaces* **2017**, *9*, 26134.
- [26] N. D. Chuong, T. D. Thanh, N. H. Kim, J. H. Lee, *ACS Appl. Mater. Interfaces* **2018**, *10*, 24523.
- [27] X. Yang, A.-Y. Lu, Y. Zhu, M. N. Hedhili, S. Min, K.-W. Huang, Y. Han, L.-J. Li, *Nano Energy* **2015**, *15*, 634.
- [28] G. Guo, Y. Guo, H. Tan, H. Yu, W. Chen, E. Fong, Q. Yan, *J. Mater. Chem. A* **2016**, *4*, 10893.
- [29] J. Xi, Y. Xia, Y. Xu, J. Xiao, S. Wang, *Chem. Commun.* **2015**, *51*, 10479.

- [30] X. Cheng, S. Dou, G. Qin, B. Wang, P. Yan, T. T. Isimjan, X. Yang, *Int. J. Hydrogen Energy* **2020**, *45*, 6128.
- [31] H. Li, X. Zhao, H. Liu, S. Chen, X. Yang, C. Lv, H. Zhang, X. She, D. Yang, *Small* **2018**, *14*, 1802824.
- [32] F. Yang, X. Chen, Z. Li, D. Wang, L. Liu, J. Ye, *ACS Appl. Energy Mater.* **2020**, *3*, 3577.
- [33] Z. Niu, C. Qiu, J. Jiang, L. Ai, *ACS Sustainable Chem. Eng.* **2019**, *7*, 2335.
- [34] H. Xia, Z. Huang, C. Lv, C. Zhang, *ACS Catal.* **2017**, *7*, 8205.
- [35] a) T. Zhou, Y. Du, D. Wang, S. Yin, W. Tu, Z. Chen, A. Borgna, R. Xu, *ACS Catal.* **2017**, *7*, 6000; b) X. Fang, L. Jiao, R. Zhang, H.-L. Jiang, *ACS Appl. Mater. Interfaces* **2017**, *9*, 23852; c) J. Zhang, K. Hou, Q. Yao, C. Wu, M. Huang, L. Guan, *Int. J. Hydrogen Energy* **2019**, *44*, 11684; d) Y. Huang, R. Yang, G. Anandhababu, J. Xie, J. Lv, X. Zhao, X. Wang, M. Wu, Q. Li, Y. Wang, *ACS Energy Lett.* **2018**, *3*, 1854; e) Y. Z. Jin, Z. Li, J. Q. Wang, R. Li, Z. Q. Li, H. Liu, J. Mao, C. K. Dong, J. Yang, S. Z. Qiao, X. W. Du, *Adv. Energy Mater.* **2018**, *8*, 1703469; f) Y. Zhang, Q. Shao, Y. Pi, J. Guo, X. Huang, *Small* **2017**, *13*, 1700355; g) Y. Wang, Y. Zhang, Z. Liu, C. Xie, S. Feng, D. Liu, M. Shao, S. Wang, *Angew. Chem. Int. Ed.* **2017**, *56*, 5867; h) J. Liu, Y. Zheng, Z. Wang, Z. Lu, A. Vasileff, S.-Z. Qiao, *Chem. Commun.* **2018**, *54*, 463; i) P. Babar, A. Lokhande, H. H. Shin, B. Pawar, M. G. Gang, S. Pawar, J. H. Kim, *Small* **2018**, *14*, 1702568.
- [36] M. Chauhan, K. P. Reddy, C. S. Gopinath, S. DeKa, *ACS Catal.* **2017**, *7*, 5871.
- [37] T. Ouyang, X.-T. Wang, X.-Q. Mai, A.-N. Chen, Z.-Y. Tang, Z.-Q. Liu, *Angew. Chem., Int. Ed.* **2020**, *59*, 11948.
- [38] C. Luan, G. Liu, Y. Liu, L. Yu, Y. Wang, Y. Xiao, H. Qiao, X. Dai, X. Zhang, *ACS Nano* **2018**, *12*, 3875.
- [39] M. Wang, W. Fu, L. Du, Y. Wei, P. Rao, L. Wei, X. Zhao, Y. Wang, S. Sun, *Appl. Surf. Sci.* **2020**, *515*, 146059.
- [40] B. Wang, H. Huang, T. Sun, P. Yan, T. T. Isimjan, J. Tian, X. Yang, *J. Colloid Interface Sci.* **2020**, *567*, 339.
- [41] G. Zhao, K. Rui, S. X. Dou, W. Sun, *Adv. Funct. Mater.* **2018**, *28*, 1803291.
- [42] a) X. Luo, P. Ji, P. Wang, R. Cheng, D. Chen, C. Lin, J. Zhang, J. He, Z. Shi, N. Li, S. Xiao, S. Mu, *Adv. Energy Mater.* **2020**, *10*, 1903891; b) H. Zhang, A. W. Maijenburg, X. Li, S. L. Schweizer, R. B. Wehrspohn, *Adv. Funct. Mater.* **2020**, *30*, 2003261.
- [43] H. Zhou, F. Yu, Q. Zhu, J. Sun, F. Qin, L. Yu, J. Bao, Y. Yu, S. Chen, Z. Ren, *Energy Environ. Sci.* **2018**, *11*, 2858.
- [44] P. Yan, M. Huang, B. Wang, Z. Wan, M. Qian, H. Yan, T. T. Isimjan, J. Tian, X. Yang, *J. Energy Chem.* **2020**, *47*, 299.